Appl. Math. Mech. -Engl. Ed., **43**(12), 1841–1856 (2022)

APPLIED MATHEMATICS AND MECHANICS (ENGLISH EDITION)

https://doi.org/10.1007/s10483-022-2927-6

Transient analysis on surface heated piezoelectric semiconductor plate lying on rigid substrate*

Luke ZHAO, Sen GU, Yaqin SONG, Feng JIN†

State Key Laboratory for Strength and Vibration of Mechanical Structures,
School of Aerospace Engineering, Xi'an Jiaotong University,
Xi'an 710049, China

(Received May 7, 2022 / Revised Sept. 5, 2022)

Abstract Based on the thermo-electro-elastic coupling theory, the mathematical model for a surface heated piezoelectric semiconductor (PS) plate is developed in the time domain. Applying the direct and inverse Laplace transformations to the established model, the mechanical and electrical responses are investigated. The comparison between the analytical solution and the finite element method (FEM) is conducted, which illustrates the validity of the derivation. The calculated results show that the maximum values of the mechanical and electrical fields appear at the heating surface. Importantly, the perturbation carriers tend to concentrate in the zone near the heating surface under the given boundary conditions. It can also be observed that the heating induced elastic wave leads to jumps for the electric potential and perturbation carrier density at the wavefront. When the thermal relaxation time is introduced, all the field quantities become smaller because of the thermal lagging effect. Meanwhile, it can be found that the thermal relaxation time can describe the smooth variation at the jump position. Besides, for a plate with P-N junction, the effect of the interface position on the electrical response is studied. The effects of the initial carrier density on the electrical properties are discussed in detail. The conclusions in this article can be the guidance for the design of PS devices serving in thermal environment.

Key words thermo-electro-elastic coupling, piezoelectric semiconductor (PS), surface heating, transient analysis

Chinese Library Classification O343.6
2010 Mathematics Subject Classification 82D37

1 Introduction

In recent years, a growing number of studies on piezoelectric semiconductor (PS) have been successfully carried out. Driven by external load, the carrier transportation in PS can be adjusted due to the coupling between piezoelectricity and semiconduction[1–2]. As applications,

* Citation: ZHAO, L. K., GU, S., SONG, Y. Q., and JIN, F. Transient analysis on surface heated piezoelectric semiconductor plate lying on rigid substrate. *Applied Mathematics and Mechanics* (*English Edition*), **43**(12), 1841–1856 (2022) https://doi.org/10.1007/s10483-022-2927-6

† Corresponding author, E-mail: jinfengzhao@263.net

Project supported by the National Natural Science Foundation of China (Nos. 12072253 and 62074125)

PS has been fabricated into many functional devices, e.g., nanogenerators, field effect transistors, sensors, and logic calculation devices[3–6]. With the development of synthetic technology, PS structures can be manufactured conveniently[7]. Thereby, PS possesses great potential in the field of smart devices.

In order to reveal how external load adjusts the carrier redistribution, one-dimensional (1D) theoretical models were established. Zhang et al.[8–9] investigated the extension of ZnO nanofibers theoretically, and revealed the distribution rules of the electromechanical fields and the carrier concentrations. Zhang et al.[10] studied the bending of a cantilever ZnO fiber under the transverse end force, and found that the electric potential and electron concentration varied rapidly near the fixed end but nearly kept constant for the other parts. In these studies, the linearized theory was adopted. Actually, the equations for PS are originally nonlinear. In some particular situations, e.g., large deformation, the linearized theory is not suitable to explain the electromechanical properties in PS. To overcome the shortcoming of the linearized theory, Yang et al.[11] utilized the perturbation solutions to analyze the nonlinearity for PS fiber. Zhao et al.[12] introduced the homotopy analysis method to study the nonlinear behavior in PS. With the consideration of nonlinearity, the internal mechanism how the external load adjusts the carriers could be described accurately. Apart from static extension or bending, dynamic response is also significant. Li et al.[13] and Wang et al.[14] found that the energy conversion efficiency was sensitive to the semiconduction in PS fiber driven by harmonic force, and the energy conversion efficiency was reduced because of the screening effect.

In view of the elementary block in integrated circuit, the P-N junction between p-type and n-type PS has also been studied. Luo et al.[15–16] and Fan et al.[17] investigated the electromechanical fields near the P-N junction. For P-N junction, potential barrier and well are important characteristics adjusting the electric conduction. It has been found that the similar function can be realized by applying distributed stress or manipulating nonhomogeneous doping density. Fan et al.[18] applied piecewise-stresses in ZnO fiber to produce potential barrier and well. Yang et al.[19] adopted nonuniform doping to produce potential barrier in PS fiber. To further explain the physical mechanism of PS, Yang et al.[20] studied the mechanical load tuned electronic energy band properties.

The composite fiber, whose material proportion can be adjusted conveniently, has been taken into account by many researchers. Cheng et al.[21] and Luo et al.[22] illustrated the interaction of piezoelectricity and semiconduction in composite PS fiber by composing piezoelectric dielectrics and non-piezoelectric semiconductors, and concluded that there was a peak value of material proportion which could produce the maximum electric potential and the most carriers. Therefore, adopting composite structure could be an efficient approach to obtaining ideal electrical responses according to the requirements. For application, Yang et al.[23] set P-N junction in composite PS fiber, and studied the electro-elastic properties in composite PS. More recently, the multiferroic coupled composite structure was proposed. Cheng et al.[24] introduced the concept of designing magneto-electro-semiconductor composite fiber, and established the multiphysical field coupling theory, in which the multiferroic coupled composite structure enabled the magnetic field to adjust the carrier transportation. Liang et al.[25] achieved the potential barrier and well by applying local magnetic field. Kong et al.[26] manipulated the piezotronic behaviors in multiferroic semiconductors through applying time-dependent magnetic field.

Besides load or magnetic field, because of the pyroelectricity and thermoelectricity in PS, temperature change can also drive the movement of carriers. Cheng et al.[27] revealed the relation between the temperature change and the carrier redistribution. By introducing the concept of composite fiber, Cheng et al.[28] studied the effect of temperature on the mobile charge in composite fiber. Cheng et al.[29–30] investigated the electrical behaviors of P-N junction and nonuniform temperature induced potential barrier and well. Yang et al.[31] analyzed the electromechanical and piezotronic behaviors in a composite PS cylindrical shell subject to thermal load. Although the temperature effect is undesirable in some situations, e.g., heat generation in

electronic devices, the studies on temperature effect is meaningful to improve the performance of devices, e.g., exploring effective cooling measures. By contrast, temperature change could be useful to generate power, e.g., thermoelectric generator[32] and solar cell[33]. Thereby, the studies on thermal coupling problems in PS are valuable for thermoelectric devices.

The studies on the interaction between temperature and carriers remind us that the temperature is an important factor for adjusting the carrier transportation. However, to date, the researchers treated temperature changes as constants. Actually, the heating process is closely related to time. Deep study on transient problems can help us understand the internal mechanism of the thermo-electro-elastic coupling properties thoroughly. Motivated by this, this article mainly concerns on the transient problem for the thermo-electro-elastic coupling properties in PS body.

The paper is arranged as follows. The theory on PS is reviewed within generalized thermoelasticity in Section 2, and a 1D theoretical model for PS plate subject to heating at the surface is developed in Section 3. Applying the direct Laplace transformation, the analytical solutions are derived. In Section 4, the field quantities in the time domain are obtained by adopting numerical inverse transformation. In Section 5, selecting specific materials, the mechanical and electrical responses are investigated and discussed. As a summary, some conclusions are drawn in Section 6.

2 Generalized thermoelastic theory for PS

The thermoelastic theory, which describes the thermal coupling properties in a medium, is necessary in our work. It has been found that the classical Fourier heat conduction theory, which treats the thermal wave propagation at an infinite speed, is unreasonable. To revise the defect of the Fourier heat conduction theory, the Cattaneo-Vernotte (C-V) heat conduction function is proposed. Furthermore, a generalized thermoelasticity theory is established by Lord and Shulman[34] (L-S theory). By introducing two thermal relaxation time, Green and Lindsay[35] proposed another new thermoelasticity theory (G-L theory). As two representative generalized thermoelastic theories, they have been widely adopted to investigate thermo-elastic coupling problems, e.g., thermal shock[36] and wave propagation[37]. Chandrasekharaiah[38–39] proposed a temperature-rate-dependent thermopiezoelectricity theory. Based on this, a great number of studies have been carried out, e.g., the thermal shock for an electromagnetic medium[40] and the dynamic response for a piezoelectric plate[41]. It should be noted that Wauer and Suherman[42] and Sladek et al.[43] explored the generalized thermoelastic theory for PS. With the help of this theory, our work can be performed conveniently.

Theoretically, the thermal coupled theory for PS consists of piezoelectricity, generalized thermoelasticity, and drift-diffusion of carriers in semiconductor. The multi-field coupling properties are described by the motion equation, Gauss's law, energy equation, and the conservation of charge for electrons and holes[8,42–43] as follows:

$$T_{ij,i} = \rho \ddot{u}_j, \tag{1a}$$

$$D_{i,i} = q(p - n + N_{\mathrm{D}}^{+} - N_{\mathrm{A}}^{-}), \tag{1b}$$

$$h_{i,i} = -T_0 \dot{\eta}, \tag{1c}$$

$$J_{i,i}^{p} = -q\dot{p}, \tag{1d}$$

$$J_{i,i}^{n} = q\dot{n}, \tag{1e}$$

where T_{ij} is the stress tensor. ρ is the mass density. u_i is the mechanical displacement tensor. D_i is the electric displacement tensor. q is the electronic charge. p and n are the concentrations of holes and electrons, respectively. N_{D}^{+} and N_{A}^{-} are the concentrations of donor and accepter impurities, respectively. J_i^p and J_i^n are the hole and electron current densities, respectively.

Besides, for the equation of energy conservation, h_i is the heat flux vector within the material, η is the entropy density, and T_0 is the initial reference temperature. The superscript of dot denotes a time derivative, and the repeated subscripts mean summation operation.

The corresponding constitutive equations describing the thermo-electro-elastic coupled behaviors in PS is

$$\begin{cases} T_{ij} = c_{ijkl}S_{kl} - e_{kij}E_k - \alpha_{ij}\theta, \quad D_i = e_{ikl}S_{kl} + \varepsilon_{ik}E_k + \beta_i\theta, \\ \eta = \alpha_{kl}S_{kl} + \beta_k E_k + \dfrac{\rho C_E}{T_0}\theta, \end{cases} \tag{2}$$

where c_{ijkl} is the elastic stiffness, e_{kij} is the piezoelectric constant, ε_{ik} is the dielectric constant, θ is the increment of temperature, α_{ij} is the thermal stress modulus, and β_i is the pyroelectric modulus. C_E is the specific heat at constant deformation. S_{kl} and E_k are the strain and electric fields, and can be expressed by the displacement u_i and the electric potential φ through

$$S_{kl} = \frac{1}{2}(u_{k,l} + u_{l,k}), \quad E_k = -\varphi_{,k}. \tag{3}$$

According to the L-S generalized thermoelastic theory[34,42–43], the heat conduction equation is formulated as

$$h_i + \tau\dot{h}_i = -k_{ij}\theta_{,j}, \tag{4}$$

where τ is the thermal relaxation time. When $\tau = 0$, the Fourier heat conduction function can be obtained. For semiconductor, the drift-diffusion theory of carriers is commonly used. It is mathematically described as[44]

$$J_i^p = qp\mu_{ij}^p E_j - qd_{ij}^p p_{,j}, \quad J_i^n = qn\mu_{ij}^n E_j + qd_{ij}^n n_{,j}, \tag{5}$$

where μ_{ij}^p (μ_{ij}^n) and d_{ij}^p (d_{ij}^n) represent the carrier mobility and carrier diffusion constants of holes (electrons), respectively. The nonlinear terms are contained in Eq. (5). For simplification, assume that $p = p_0 + \Delta p$ and $n = n_0 + \Delta n$, in which $\Delta p\,(\Delta n)$ is the perturbation of holes (electrons), and $p_0\,(n_0)$ is treated as uniform doping, i.e., $p_0 = N_{\rm A}^-$ ($n_0 = N_{\rm D}^+$). Furthermore, Eq. (1b) and Eq. (5) can be approximated by

$$D_{i,i} = q(\Delta p - \Delta n), \quad J_i^p \cong qp_0\mu_{ij}^p E_j - qd_{ij}^p \Delta p_{,j}, \quad J_i^n \cong qn_0\mu_{ij}^n E_j + qd_{ij}^n \Delta n_{,j}. \tag{6}$$

With the linearized equations, the mechanical and electrical responses for temperature coupled PS under thermal load can be studied analytically.

3 Formulation for the surface heating PS plate

The system, which consists of substrate and covered layers, is a kind of commonly used elementary structure in smart devices. According to the requirements in applications, the substrate could be elastic or rigid[45]. Herein, two typical plates lying on a rigid substrate are taken into account (see Fig. 1). In both cases, the plates are infinite along the x_1- and x_2-directions. Along the x_3-direction, the plates are heated at the upper surface ($x_3 = 0$), and fixed at

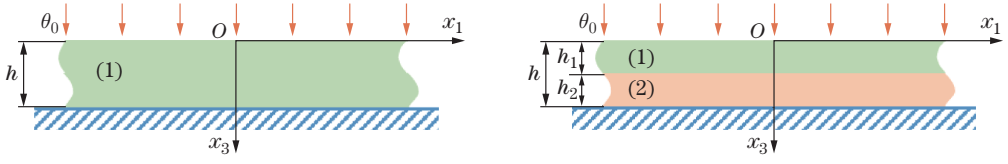

(a) Case 1 (b) Case 2

Fig. 1 Sketch for the surface heating PS plate (color online)

the bottom surface ($x_3 = h$). The polarization direction is along positive x_3. For Case 2, the thicknesses for the two layers are h_1 and h_2, respectively. It should be noted that the materials for the two layers are identical but with different initial carrier densities. Mathematically, the discontinuity of the initial carrier densities along the x_3-direction is described as

$$n_0(p_0) = \begin{cases} n_0^{(1)}(p_0^{(1)}), & 0 < x_3 \leqslant h_1, \\ n_0^{(2)}(p_0^{(2)}), & h_1 < x_3 \leqslant h_2, \end{cases}$$

where $n_0^{(1)}(p_0^{(1)})$ and $n_0^{(2)}(p_0^{(2)})$ stand for the artificially adjusted initial carrier densities for the first layer and the second layer, respectively. In view of this, we focus on the electro-elastic properties of the P-N junction in Case 2.

Consider a homogeneous heating source, independent of the x_1- and x_2-directions. In this situation, the 1D model along the x_3-direction can be adopted to describe the thermo-electro-elastic coupling properties for the given cases. Correspondingly, the constitutive equations for the ith layer are simplified to

$$\begin{cases} T_{33}^{(i)} = c_{33}^{(i)} S_{33}^{(i)} - e_{33}^{(i)} E_3^{(i)} - \alpha_{33}^{(i)} \theta^{(i)}, \quad D_3^{(i)} = e_{33}^{(i)} S_{33}^{(i)} + \varepsilon_{33}^{(i)} E_3^{(i)} + \beta_3^{(i)} \theta^{(i)}, \\ \eta^{(i)} = \alpha_{33}^{(i)} S_{33}^{(i)} + \beta_3^{(i)} E_3^{(i)} + \dfrac{\rho^{(i)} C_E^{(i)}}{T_0} \theta^{(i)}, \quad J_3^{p(i)} = q p_0^{(i)} \mu_{33}^{p(i)} E_3^{(i)} - q d_{33}^{p(i)} \Delta p_{,3}^{(i)}, \\ J_3^{n(i)} = q n_0^{(i)} \mu_{33}^{n(i)} E_3^{(i)} + q d_{33}^{n(i)} \Delta n_{,3}^{(i)}. \end{cases} \tag{7}$$

Substituting Eq. (7) into the linearized governing equations yields 1D equations as follows:

$$c_{33}^{(i)} u_{3,33}^{(i)} + e_{33}^{(i)} \varphi_{,33}^{(i)} - \alpha_{33}^{(i)} \theta_{,3}^{(i)} = \rho^{(i)} \ddot{u}_3^{(i)}, \tag{8a}$$

$$e_{33}^{(i)} u_{3,33}^{(i)} - \varepsilon_{33}^{(i)} \varphi_{,33}^{(i)} + \beta_3^{(i)} \theta_{,3}^{(i)} = q(\Delta p^{(i)} - \Delta n^{(i)}), \tag{8b}$$

$$- k_{33}^{(i)} \theta_{,33}^{(i)} + \left(1 + \tau^{(i)} \frac{\partial}{\partial t}\right)(T_0 \alpha_{33}^{(i)} \dot{u}_{3,3}^{(i)} - T_0 \beta_3^{(i)} \dot{\varphi}_{,3}^{(i)} + \rho^{(i)} C_E^{(i)} \dot{\theta}^{(i)}) = 0, \tag{8c}$$

$$- q p_0^{(i)} \mu_{33}^{p(i)} \varphi_{,33}^{(i)} - q d_{33}^{p(i)} \Delta p_{,33}^{(i)} = -q \Delta \dot{p}^{(i)}, \tag{8d}$$

$$- q n_0^{(i)} \mu_{33}^{n(i)} \varphi_{,33}^{(i)} + q d_{33}^{n(i)} \Delta n_{,33}^{(i)} = q \Delta \dot{n}^{(i)}. \tag{8e}$$

When the temperature-related terms are dropped ($\theta^{(i)}$ and Eq. (8c)), Eqs. (8a), (8b), (8c), (8d), and (8e) degenerate to the equation describing pure PS as in Ref. [8].

For qualitative analysis, the following non-dimensional qualities are introduced:

$$\begin{cases} \xi = \dfrac{x_3}{h}, \quad \bar{t}^{(i)} = t^{(i)} \sqrt{\dfrac{c_{33}^{(i)}}{\rho^{(i)} h^2}}, \quad \overline{u}^{(i)} = \dfrac{u_3^{(i)}}{h}, \quad \overline{\varphi}^{(i)} = \dfrac{\varepsilon_{33}^{(i)}}{e_{33}^{(i)} h} \varphi^{(i)}, \quad \overline{\theta}^{(i)} = \dfrac{\beta_3^{(i)}}{e_{33}^{(i)}} \theta^{(i)}, \\ \overline{n}^{(i)} = \dfrac{qh}{e_{33}^{(i)}} \Delta n^{(i)}, \quad \overline{p}^{(i)} = \dfrac{qh}{e_{33}^{(i)}} \Delta p^{(i)}, \quad \overline{T}^{(i)} = \dfrac{T_{33}^{(i)}}{c_{33}^{(i)}}, \quad \overline{D}^{(i)} = \dfrac{D_3^{(i)}}{e_{33}^{(i)}}, \quad \overline{J}^{n(i)} = \dfrac{J_3^{n(i)} h^2}{e_{33}^{(i)} d_{33}^{n(i)}}, \\ \overline{J}^{p(i)} = \dfrac{J_3^{p(i)} h^2}{e_{33}^{(i)} d_{33}^{p(i)}}, \quad a_1^{(i)} = \dfrac{e_{33}^{(i)2}}{\varepsilon_{33}^{(i)} c_{33}^{(i)}}, \quad a_2^{(i)} = \dfrac{\alpha_{33}^{(i)} e_{33}^{(i)}}{c_{33}^{(i)} \beta_3^{(i)}}, \quad a_3^{(i)} = \dfrac{\beta_3^{(i)} T_0 \alpha_{33}^{(i)} h}{e_{33}^{(i)} k_{33}^{(i)}} \sqrt{\dfrac{c_{33}^{(i)}}{\rho^{(i)}}}, \\ a_4^{(i)} = \dfrac{\beta_3^{(i)2} T_0 h}{\varepsilon_{33}^{(i)} k_{33}^{(i)}} \sqrt{\dfrac{c_{33}^{(i)}}{\rho^{(i)}}}, \quad a_5^{(i)} = \dfrac{\rho^{(i)} C_E^{(i)} h}{k_{33}^{(i)}} \sqrt{\dfrac{c_{33}^{(i)}}{\rho^{(i)}}}, \quad a_6^{(i)} = \dfrac{q p_0^{(i)} \mu_{33}^{p(i)} h^2}{d_{33}^{p(i)} \varepsilon_{33}^{(i)}}, \quad a_7^{(i)} = \dfrac{h}{d_{33}^{p(i)}} \sqrt{\dfrac{c_{33}^{(i)}}{\rho^{(i)}}}, \\ a_8^{(i)} = \dfrac{q n_0^{(i)} \mu_{33}^{n(i)} h^2}{d_{33}^{n(i)} \varepsilon_{33}^{(i)}}, \quad a_9^{(i)} = \dfrac{h}{d_{33}^{n(i)}} \sqrt{\dfrac{c_{33}^{(i)}}{\rho^{(i)}}}, \quad \overline{\tau}^{(i)} = \tau^{(i)} \sqrt{\dfrac{\rho^{(i)} h}{c_{33}^{(i)}}}. \end{cases}$$

It should be noted that $\bar{t}^{(1)} = \bar{t}^{(2)} = \bar{t}$ due to the same material for the two layers in Case 2. After non-dimensional transformation, the governing equations are rewritten as

$$\overline{u}^{(i)}_{,\xi\xi} + a_1^{(i)}\overline{\varphi}^{(i)}_{,\xi\xi} - a_2^{(i)}\overline{\theta}^{(i)}_{,\xi} = \overline{u}^{(i)}_{,\bar{t}\bar{t}}, \tag{9a}$$

$$\overline{u}^{(i)}_{,\xi\xi} - \overline{\varphi}^{(i)}_{,\xi\xi} + \overline{\theta}^{(i)}_{,\xi} = \overline{p}^{(i)} - \overline{n}^{(i)}, \tag{9b}$$

$$-\overline{\theta}^{(i)}_{,\xi\xi} + \Big(1 + \overline{\tau}^{(i)}\frac{\partial}{\partial\bar{t}}\Big)(a_3^{(i)}\overline{u}_{,\xi\bar{t}} - a_4^{(i)}\overline{\varphi}^{(i)}_{,\xi\bar{t}} + a_5^{(i)}\overline{\theta}^{(i)}_{,\bar{t}}) = 0, \tag{9c}$$

$$a_6^{(i)}\overline{\varphi}^{(i)}_{,\xi\xi} + \overline{p}^{(i)}_{,\xi\xi} = a_7^{(i)}\overline{p}^{(i)}_{,\bar{t}}, \tag{9d}$$

$$-a_8^{(i)}\overline{\varphi}^{(i)}_{,\xi\xi} + \overline{n}^{(i)}_{,\xi\xi} = a_9^{(i)}\overline{n}^{(i)}_{,\bar{t}}\,. \tag{9e}$$

With the help of boundary conditions, the solutions could be unique for the governing equations. In Case 1, n-type semiconductor is considered only. The governing equations are consist of Eqs. (9a), (9b), (9c), and (9e) by ignoring $\overline{p}$. The boundary conditions are

$$\begin{cases} \overline{T}^{(1)}(0) = 0, \quad \overline{D}^{(1)}(0) = 0, \quad \overline{J}^{n(1)}(0) = 0, \quad \overline{\theta}^{(1)}(0) = \overline{\theta}_0, \\ \overline{u}^{(1)}(1) = 0, \quad \overline{\varphi}^{(1)}(1) = 0, \quad \overline{n}^{(1)}(1) = 0, \quad \overline{\theta}^{(1)}_{,\xi}(1) = 0. \end{cases} \tag{10}$$

For Case 2, not only the boundary conditions but also the continuity conditions are needed. The boundary conditions are

$$\begin{cases} \overline{T}^{(1)}(0) = 0, \quad \overline{D}^{(1)}(0) = 0, \quad \overline{J}^{n(1)}(0) = 0, \quad \overline{J}^{p(1)}(0) = 0, \quad \overline{\theta}^{(1)}(0) = \overline{\theta}_0, \\ \overline{u}^{(2)}(1) = 0, \quad \overline{\varphi}^{(2)}(1) = 0, \quad \overline{n}^{(2)}(1) = 0, \quad \overline{p}^{(2)}(1) = 0, \quad \overline{\theta}^{(2)}_{,\xi}(1) = 0. \end{cases} \tag{11}$$

The continuity conditions are

$$\begin{cases} \overline{T}^{(1)}(\gamma) = \overline{T}^{(2)}(\gamma), \quad \overline{D}^{(1)}(\gamma) = \overline{D}^{(2)}(\gamma), \quad \overline{J}^{n(1)}(\gamma) = \overline{J}^{n(2)}(\gamma), \quad \overline{J}^{p(1)}(\gamma) = \overline{J}^{p(2)}(\gamma), \\ \overline{u}^{(1)}(\gamma) = \overline{u}^{(2)}(\gamma), \quad \overline{\varphi}^{(1)}(\gamma) = \overline{\varphi}^{(2)}(\gamma), \quad \overline{n}^{(1)}(\gamma) = \overline{n}^{(2)}(\gamma), \quad \overline{p}^{(1)}(\gamma) = \overline{p}^{(2)}(\gamma), \\ \overline{\theta}^{(1)}(\gamma) = \overline{\theta}^{(2)}(\gamma), \quad \overline{\theta}^{(1)}_{,\xi}(\gamma) = \overline{\theta}^{(2)}_{,\xi}(\gamma), \end{cases} \tag{12}$$

where $\gamma = h_1/h$ is introduced to manipulate the thickness ratio. The above derivations describe the thermo-electro-elastic coupling model for the surface heating plate in the time domain. To reveal the mechanical and electrical properties in PS, a proper solution should be sought. In the following, the solution will be discussed in detail.

4 Solutions for the thermo-electro-elastic coupling model

4.1 Solutions in the Laplace domain

Practically, let the range of time $\bar{t}$ be $(0, +\infty)$. The direct Laplace transformation helps us to obtain the solutions in the Laplace domain. Then, the inverse Laplace transformation can be adopted to calculate the real solutions in the time domain. Applying the Laplace transformation

$$L(f(\bar{t})) = \widetilde{f}(s) = \int_0^{+\infty} f(\bar{t})\exp(-s\bar{t})\mathrm{d}\bar{t}$$

to Eqs. (9a)–(12) yields the governing equations in the Laplace domain as follows:

$$\widetilde{\overline{u}}^{(i)}_{,\xi\xi} + a_1^{(i)}\widetilde{\overline{\varphi}}^{(i)}_{,\xi\xi} - a_2^{(i)}\widetilde{\overline{\theta}}^{(i)}_{,\xi} = s^2\widetilde{\overline{u}}^{(i)}, \tag{13a}$$

$$\widetilde{\overline{u}}^{(i)}_{,\xi\xi} - \widetilde{\overline{\varphi}}^{(i)}_{,\xi\xi} + \widetilde{\overline{\theta}}^{(i)}_{,\xi} = \widetilde{\overline{p}}^{(i)} - \widetilde{\overline{n}}^{(i)}, \tag{13b}$$

$$-\widetilde{\overline{\theta}}^{(i)}_{,\xi\xi} + s(1+\overline{\tau}^{(i)}s)(a_3^{(i)}\widetilde{\overline{u}}^{(i)}_{,\xi} - a_4^{(i)}\widetilde{\overline{\varphi}}^{(i)}_{,\xi} + a_5^{(i)}\widetilde{\overline{\theta}}^{(i)}) = 0, \tag{13c}$$

$$a_6^{(i)}\widetilde{\overline{\varphi}}^{(i)}_{,\xi\xi} + \widetilde{\overline{p}}^{(i)}_{,\xi\xi} = sa_7^{(i)}\widetilde{\overline{p}}^{(i)}, \tag{13d}$$

$$-a_8^{(i)}\widetilde{\overline{\varphi}}^{(i)}_{,\xi\xi} + \widetilde{\overline{n}}^{(i)}_{,\xi\xi} = sa_9^{(i)}\widetilde{\overline{n}}^{(i)}. \tag{13e}$$

The boundary conditions for Case 1 are rewritten as

$$\begin{cases} \widetilde{\overline{T}}^{(1)}(0) = 0, \quad \widetilde{\overline{D}}^{(1)}(0) = 0, \quad \widetilde{\overline{J}}^{n(1)}(0) = 0, \quad \widetilde{\overline{\theta}}^{(1)}(0) = \widetilde{\overline{\theta}}_0, \\ \widetilde{\overline{u}}^{(1)}(1) = 0, \quad \widetilde{\overline{\varphi}}^{(1)}(1) = 0, \quad \widetilde{\overline{n}}^{(1)}(1) = 0, \quad \widetilde{\overline{\theta}}^{(1)}_{,\xi}(1) = 0. \end{cases} \tag{14}$$

The boundary conditions and continuity conditions for Case 2 are, respectively, rewritten as

$$\begin{cases} \widetilde{\overline{T}}^{(1)}(0) = 0, \quad \widetilde{\overline{D}}^{(1)}(0) = 0, \quad \widetilde{\overline{J}}^{n(1)}(0) = 0, \quad \widetilde{\overline{J}}^{p(1)}(0) = 0, \quad \widetilde{\overline{\theta}}^{(1)}(0) = \widetilde{\overline{\theta}}_0, \\ \widetilde{\overline{u}}^{(2)}(1) = 0, \quad \widetilde{\overline{\varphi}}^{(2)}(1) = 0, \quad \widetilde{\overline{n}}^{(2)}(1) = 0, \quad \widetilde{\overline{p}}^{(2)}(1) = 0, \quad \widetilde{\overline{\theta}}^{(2)}_{,\xi}(1) = 0, \end{cases} \tag{15}$$

$$\begin{cases} \widetilde{\overline{T}}^{(1)}(\gamma) = \widetilde{\overline{T}}^{(2)}(\gamma), \quad \widetilde{\overline{D}}^{(1)}(\gamma) = \widetilde{\overline{D}}^{(2)}(\gamma), \quad \widetilde{\overline{J}}^{n(1)}(\gamma) = \widetilde{\overline{J}}^{n(2)}(\gamma), \quad \widetilde{\overline{J}}^{p(1)}(\gamma) = \widetilde{\overline{J}}^{p(2)}(\gamma), \\ \widetilde{\overline{u}}^{(1)}(\gamma) = \widetilde{\overline{u}}^{(2)}(\gamma), \quad \widetilde{\overline{\varphi}}^{(1)}(\gamma) = \widetilde{\overline{\varphi}}^{(2)}(\gamma), \quad \widetilde{\overline{n}}^{(1)}(\gamma) = \widetilde{\overline{n}}^{(2)}(\gamma), \quad \widetilde{\overline{p}}^{(1)}(\gamma) = \widetilde{\overline{p}}^{(2)}(\gamma), \\ \widetilde{\overline{\theta}}^{(1)}(\gamma) = \widetilde{\overline{\theta}}^{(2)}(\gamma), \quad \widetilde{\overline{\theta}}^{(1)}_{,\xi}(\gamma) = \widetilde{\overline{\theta}}^{(2)}_{,\xi}(\gamma). \end{cases} \tag{16}$$

In this article, the heating source is treated as $\overline{\theta}_0 = \Theta H(\overline{t})$, where Θ is the magnitude value, and H is the Heaviside function. Applying the Laplace transformation yields

$$\widetilde{\overline{\theta}}_0 = \frac{\Theta}{s}. \tag{17}$$

The solutions to Eqs. (13a), (13b), (13c), (13d), and (13e) are

$$\widetilde{\overline{u}}^{(i)} = A_1^{(i)}\exp(\lambda^{(i)}\xi), \tag{18a}$$

$$\widetilde{\overline{\varphi}}^{(i)} = A_2^{(i)}\exp(\lambda^{(i)}\xi), \tag{18b}$$

$$\widetilde{\overline{\theta}}^{(i)} = A_3^{(i)}\exp(\lambda^{(i)}\xi), \tag{18c}$$

$$\widetilde{\overline{p}}^{(i)} = A_4^{(i)}\exp(\lambda^{(i)}\xi), \tag{18d}$$

$$\widetilde{\overline{n}}^{(i)} = A_5^{(i)}\exp(\lambda^{(i)}\xi). \tag{18e}$$

For Case 1, substituting Eqs. (18a), (18b), (18c), (18d), and (18e) into Eqs. (13a), (13b), (13c), and (13e) leads to four linear homogeneous algebraic equations for $A_1^{(1)}$, $A_2^{(1)}$, $A_3^{(1)}$, and $A_5^{(1)}$. For nontrivial solutions, the determinant of the coefficient matrix of the equations has to vanish, which leads to a polynomial equation of degree eight for $\lambda^{(1)}$. Denote the eight roots

of the algebraic equations as $\lambda_m^{(1)}$ $(m=1,2,3,\cdots,8)$ and the nontrivial solution of $A_1^{(1)}$, $A_2^{(1)}$, $A_3^{(1)}$, and $A_5^{(1)}$ as $A_{1m}^{(1)}$, $A_{2m}^{(1)}$, $A_{3m}^{(1)}$, and $A_{5m}^{(1)}$. The solutions are expressed as

$$\begin{aligned}\begin{pmatrix}\widetilde{\overline{u}}^{(1)}\\ \widetilde{\overline{\varphi}}^{(1)}\\ \widetilde{\overline{\theta}}^{(1)}\\ \widetilde{\overline{n}}^{(1)}\end{pmatrix}&=\sum_{m=1}^{6}\begin{pmatrix}A_{1m}^{(1)}\\ A_{2m}^{(1)}\\ A_{3m}^{(1)}\\ A_{5m}^{(1)}\end{pmatrix}\exp(\lambda_m^{(1)}\xi)+\begin{pmatrix}0\\ 0\\ A_{37}^{(1)}\xi+A_{38}^{(1)}\\ 0\end{pmatrix}\\&=\sum_{m=1}^{6}\begin{pmatrix}B_{1m}^{(1)}A_{3m}^{(1)}\\ B_{2m}^{(1)}A_{3m}^{(1)}\\ A_{3m}^{(1)}\\ B_{5m}^{(1)}A_{3m}^{(1)}\end{pmatrix}\exp(\lambda_m^{(1)}\xi)+\begin{pmatrix}0\\ 0\\ A_{37}^{(1)}\xi+A_{38}^{(1)}\\ 0\end{pmatrix},\end{aligned}\tag{19}$$

where $B_{1m}^{(1)}$, $B_{2m}^{(1)}$, and $B_{5m}^{(1)}$ are derived from the governing equations. Substitute Eq. (19) into Eq. (14). Then, eight linear algebraic equations for $A_{3m}^{(1)}$ are obtained, and the solutions can be calculated.

Similarly, for Case 2, substituting Eq. (18) into Eq. (13) leads to five linear homogeneous algebraic equations for $A_1^{(i)}$, $A_2^{(i)}$, $A_3^{(i)}$, $A_4^{(i)}$, and $A_5^{(i)}$. Then, a polynomial equation of degree ten for $\lambda^{(i)}$ can be obtained. With the same variables, the solutions for both layers are expressed as

$$\begin{aligned}\begin{pmatrix}\widetilde{\overline{u}}^{(i)}\\ \widetilde{\overline{\varphi}}^{(i)}\\ \widetilde{\overline{\theta}}^{(i)}\\ \widetilde{\overline{p}}^{(i)}\\ \widetilde{\overline{n}}^{(i)}\end{pmatrix}&=\sum_{m=1}^{8}\begin{pmatrix}A_{1m}^{(i)}\\ A_{2m}^{(i)}\\ A_{3m}^{(i)}\\ A_{4m}^{(i)}\\ A_{5m}^{(i)}\end{pmatrix}\exp(\lambda_m^{(1)}\xi)+\begin{pmatrix}0\\ 0\\ A_{39}^{(i)}\xi+A_{310}^{(i)}\\ 0\\ 0\end{pmatrix}\\&=\sum_{m=1}^{8}\begin{pmatrix}C_{1m}^{(i)}A_{3m}^{(i)}\\ C_{2m}^{(i)}A_{3m}^{(i)}\\ A_{3m}^{(i)}\\ C_{4m}^{(i)}A_{3m}^{(i)}\\ C_{5m}^{(i)}A_{3m}^{(i)}\end{pmatrix}\exp(\lambda_m^{(i)}\xi)+\begin{pmatrix}0\\ 0\\ A_{39}^{(i)}\xi+A_{310}^{(i)}\\ 0\\ 0\end{pmatrix},\quad i=1,2.\end{aligned}\tag{20}$$

Substituting Eq. (20) into Eqs. (15) and (16) yields twenty linear algebraic equations for $A_{3m}^{(i)}$. Finally, the solutions for Case 2 can be calculated.

4.2 Solutions in the time domain

For the purpose of obtaining real solutions in the time domain, the inverse Laplace transformation should be performed. In view of the complexity of solutions in the Laplace domain, it is difficult to search the analytical expressions. In this work, the numerical inverse Laplace transformation proposed by Durbin[46] is adopted to calculate the real solutions in the time domain.

5 Numerical analysis and discussion

As an example, take the CdSe plate into account in the numerical analysis. The relative material parameters are[47–48]

$$\begin{cases} c_{33}^{(i)} = 83.6\,\text{GPa}, \quad e_{33}^{(i)} = 0.347\,\text{C/m}^2, \quad \varepsilon_{33}^{(i)} = 9.03\times10^{-11}\,\text{F/m}, \\ \alpha_{33}^{(i)} = 0.551\times10^{6}\,\text{N/(K}\cdot\text{m}^2), \quad \beta_3^{(i)} = -2.94\times10^{-6}\,\text{C/(K}\cdot\text{m}^2), \quad k_{33}^{(i)} = 1.4\,\text{W/(K}\cdot\text{m}), \\ \rho^{(i)} = 7\,600\,\text{kg/m}^3, \quad C_E^{(i)} = 420\,\text{J/(kg}\cdot\text{K}), \quad T_0 = 300\,\text{K}, \quad \mu_{33}^{n(i)} = 0.09\,\text{m}^2\text{/(V}\cdot\text{s}), \\ \mu_{33}^{p(i)} = 0.005\,\text{m}^2\text{/(V}\cdot\text{s}), \quad d_{33}^{n(i)} = \dfrac{k_\text{e}T}{q}\mu_{33}^{n(i)}, \quad d_{33}^{p(i)} = \dfrac{k_\text{e}T}{q}\mu_{33}^{p(i)}, \quad \dfrac{k_\text{e}T}{q} = 0.026\,\text{V}, \\ q = 1.602\times10^{-9}\,\text{C}, \quad \overline{\tau}^{(i)} = 0.05, \quad h = 100\,\text{nm}, \quad \Theta = 1. \end{cases}$$

Additionally, for Case 1, the initial carrier density is $n_0 = 10^{21}\,\text{m}^{-3}$. For Case 2, assume that $n_0^{(1)} = p_0^{(2)} = 0.5a_0$ and $n_0^{(2)} = p_0^{(1)} = a_0$.

5.1 Single layered plate subject to the surface heating source (Case 1)

Before analysis, the validity of the derivations should be proved. The finite element method (FEM) is used based on the COMSOL software, and the obtained results are shown in Fig. 2, along with the results obtained from the analytical method for comparison. It is shown that the results from the analytical solution agree well with those obtained by the FEM.

In Fig. 2(a), the temperature change $\overline{\theta}$ is 1 at the heating surface ($\xi = 0$). It verifies the correctness of the solutions further. With the prolonging of heating time, Fig. 2(b) shows that the deformation $\overline{u}$ increases near the heating surface and keeps steady in the other parts. At the same time, larger deformation induces larger electric potential $\overline{\varphi}$ (see Fig. 2(c)). Driven by the electric potential, more perturbation carriers $\overline{n}$ tend to concentrate in the zone near the heating surface (see Fig. 2(d)).

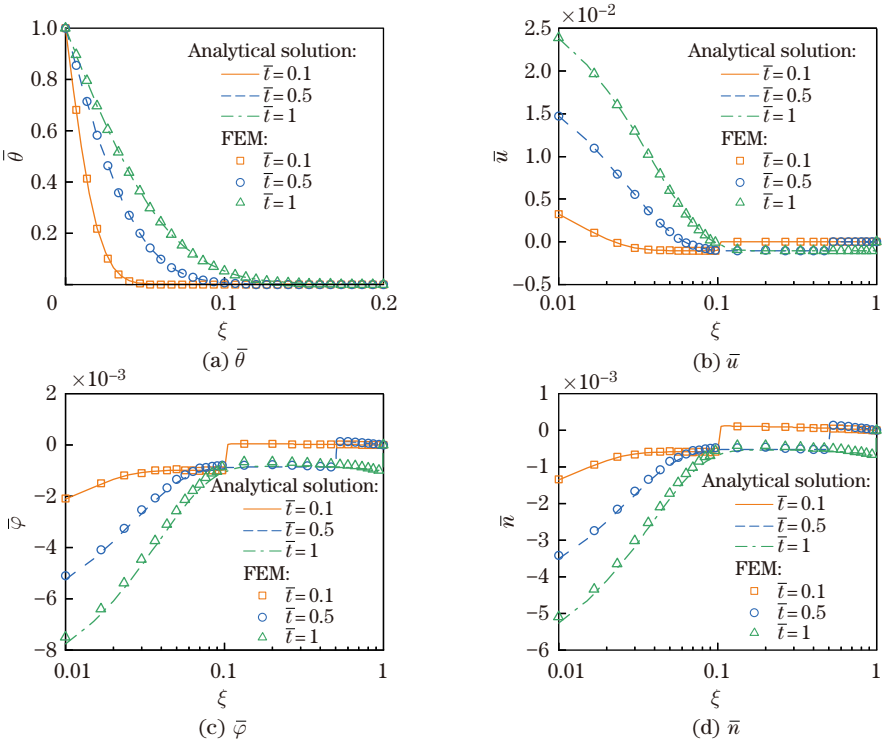

Fig. 2 Comparison of the results from the analytical method and the FEM (color online)

It can be observed that there are jumps for deformation, electric potential, and perturbation carrier density. To explain this phenomenon, Fig. 3 gives the comparison among the displacement $\overline{u}$, the stress $\overline{T}$, the electric potential $\overline{\varphi}$, the electric field $\overline{E}$, and the perturbation carrier $\overline{n}$ when $\overline{t} = 0.5$. It can be found that the jump position is very close to $\xi = 0.5$. According to the non-dimensional governing equation (Eq. (9)), the phase speed of the elastic wave in a pure elastic medium is equal to 1. Although the phase speed of the elastic wave in PS is not 1 because of the dispersion and dissipation, it still can be predicted reasonably that the jump of deformation is induced by the propagation of elastic wave according to the calculated results. Subject to the jump of deformation, a peak appears for stress. At the same position, there is a jump for the electric potential. This phenomenon can also be seen in Ref. [18], where the piecewise-stress produced electric potential barrier. Further, the sudden change for the electric field and the jump for the perturbation carrier density are produced. The above discussion illustrates that the heating induced elastic wave propagation has the ability to change the distributions of field quantities in PS.

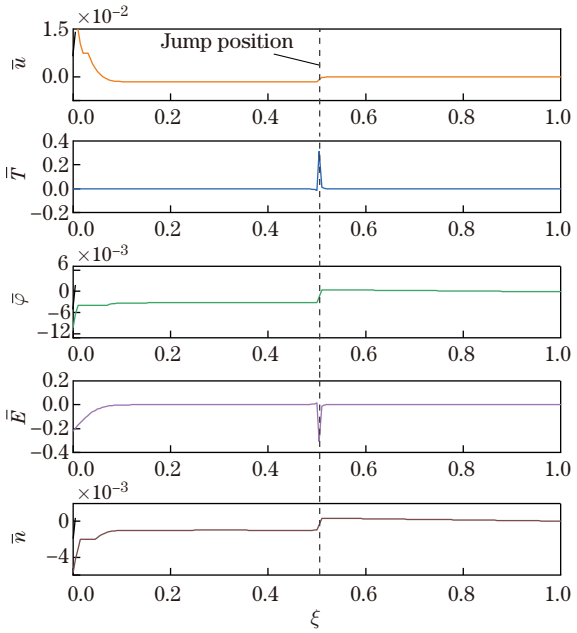

Fig. 3 Comparisons among the displacement $\overline{u}$, the stress $\overline{T}$, the electric potential $\overline{\varphi}$, the electric field $\overline{E}$, and the perturbation carrier density $\overline{n}$ when $\overline{t} = 0.5$ (color online)

In this article, the generalized thermal-elasticity (L-S theory) is considered. The thermal relaxation time $\overline{\tau}$ is an important factor describing the thermal wave propagation. According to the works carried by other researchers, it can be reasonably predicted that the thermal relaxation time is able to describe different distributions of field quantities in PS. To qualitatively illustrate the effect of the thermal relaxation time on the distributions of field quantities, two thermal relaxation time, i.e., $\overline{\tau} = 0, 0.05$, is adopted, and the calculated results are plotted in Fig. 4. It can be concluded that the effects of the thermal relaxation time on the temperature, electrical, or mechanical quantities are stronger for shorter time heating. It means that the consideration of thermal relaxation time is necessary for short time heating process. It can also be observed that when the thermal relaxation time is considered, the gentle slopes replace the abrupt jumps (see Figs. 4(b), 4(d), and 4(f)), and the maximal values at sudden changed positions for the stress and electric fields become smaller (see Figs. 4(c) and 4(e)).

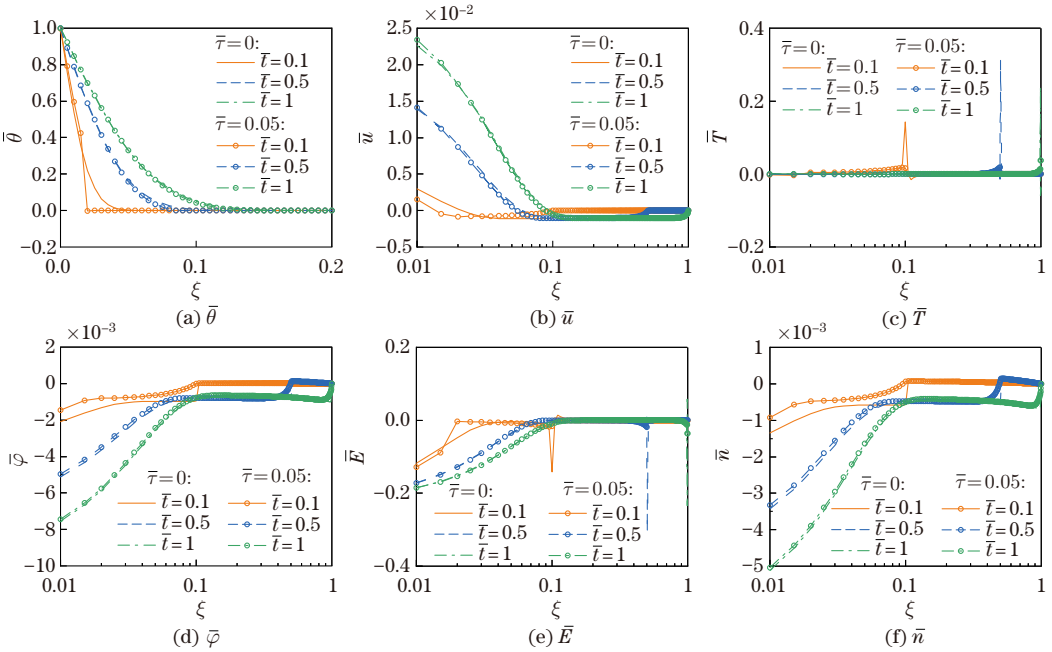

Fig. 4 Thermal relaxation time effects on the fields in PS (color online)

This is because the thermal relaxation time plays the role of damping, and the longer thermal relaxation time causes smaller values of all fields in the PS plate in short heating time.

In semiconductor structures, the initial carrier density can be adjusted artificially. The investigation about the initial carrier density effect on electrical properties is meaningful for practical application. As significant quantities, $\overline{\varphi}$ and $\overline{n}$ are studied here. Considering the thermal relaxation time (i.e., $\overline{\tau}=0.05$), the electric potential and perturbation carrier density at the heating surface (i.e., $\overline{\varphi}(0)$ and $\overline{n}(0)$) vary with the increase in the initial carrier density n_0 (see Fig. 5). It can be found that the electric potential decreases while the perturbation carrier density increases when $\overline{\tau}$ increases. The physical mechanism behind this phenomenon is that the mobile charge tends to screen the electric potential. This conclusion can also be seen in Ref. [13]. Differently, in this article, it can be concluded from Fig. 5 that the screening effect is much stronger for longer heating time. This is because more perturbation carriers are produced by longer heating time, and thus a stronger screening effect is induced.

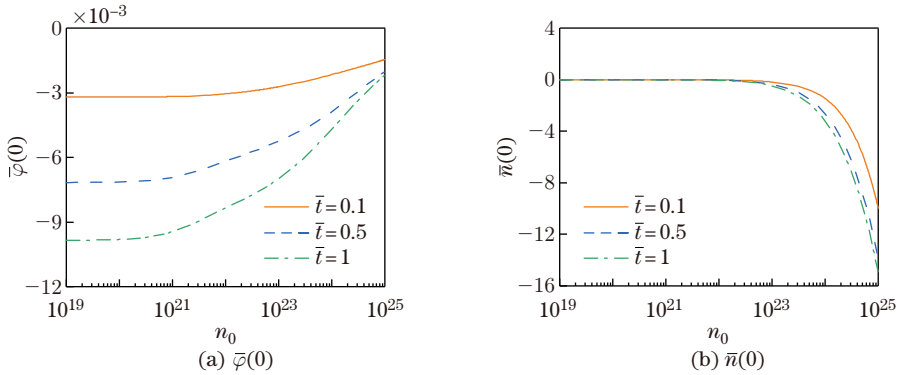

Fig. 5 Effects of the initial carrier density on the electric potential and perturbation carrier density (color online)

5.2 Double layered plate subject to the surface heating source (Case 2)

In this section, a double layered plate is focused. Herein, the electrical properties for the P-N junction between the two layers are the objects. From the calculated results in Subsection 5.1, it is found the mechanical or electrical field quantities vary quickly in the range about (0,0.1]. Consequently, the adjustment of the interface position in the range could lead to visible results. In the following discussion, $\overline{\tau} = 0.05$, $\overline{t} = 0.5$, and $a_0 = 10^{21}\,\mathrm{m}^{-3}$.

For a piezoelectric P-N junction in the equilibrium state, which is not disturbed by any external perturbation, the initial contact potential difference of the space charge zone φ_0 can be determined by the doping densities through[17,44] $\varphi_0 = (k_\mathrm{e}T/q)\ln(N_\mathrm{D}^+ N_\mathrm{A}^-/n_\mathrm{i}^2)$. Since $n_{n0} \approx N_\mathrm{D}^+$ and $n_{p0} \approx n_\mathrm{i}^2/N_\mathrm{A}^-$, $\varphi_0 = (k_\mathrm{e}T/q)\ln(n_{n0}/n_{p0})$, where n_i is the intrinsic carrier concentration, and n_{n0} and n_{p0} stand for the initial carrier concentrations of electrons in the n- and p-zones, respectively. According to the given parameters, the initial contact potential difference $\varphi_0 \approx 0.018\,\mathrm{V}$. Correspondingly, the non-dimensional initial contact potential difference $\overline{\varphi}_0$ is calculated by $\overline{\varphi}_0 = \varepsilon_{33}^{(1)}\varphi_0/(e_{33}^{(1)}h) \approx 4.69 \times 10^{-5}$.

Next, we discuss the variation of the electric potential in the non-equilibrium state. In Fig. 6(a), the interface position affected electric potential is plotted. It can be seen that the thermal induced electric potential $\overline{\varphi}$ is much larger than the initial contact potential difference $\overline{\varphi}_0$ in the equilibrium state, indicating that the potential barrier is dominated by the thermal induced electric potential. In Figs. 6(b), 6(c), and 6(d), the variations of the electric field, the perturbation carrier density of electrons, and the perturbation carrier density of holes are plotted, respectively. It can be observed that the position of the interface nearly does not affect the electric potential and electric fields. However, in the zone near the heating surface, the perturbation carrier density of electrons decreases while the perturbation carrier density of holes increases with the moving of interface. Furthermore, Figs. 6(e) and 6(f) give the polarization charge and the total charge, respectively. According to the definition, the polarization charge ρ^p can be calculated by $\rho^\mathrm{p} = -P_{3,3}$, where $P_3 = D_3 - \varepsilon_0 E_3$ is the polarization vector. According to the aforementioned non-dimensional method, the non-dimensional polarization charge is defined as $\overline{\rho}^\mathrm{p} = -\overline{D}_{,\xi} - (\varepsilon_0/\varepsilon_{33}^{(1)})\overline{\varphi}_{,\xi\xi}$.

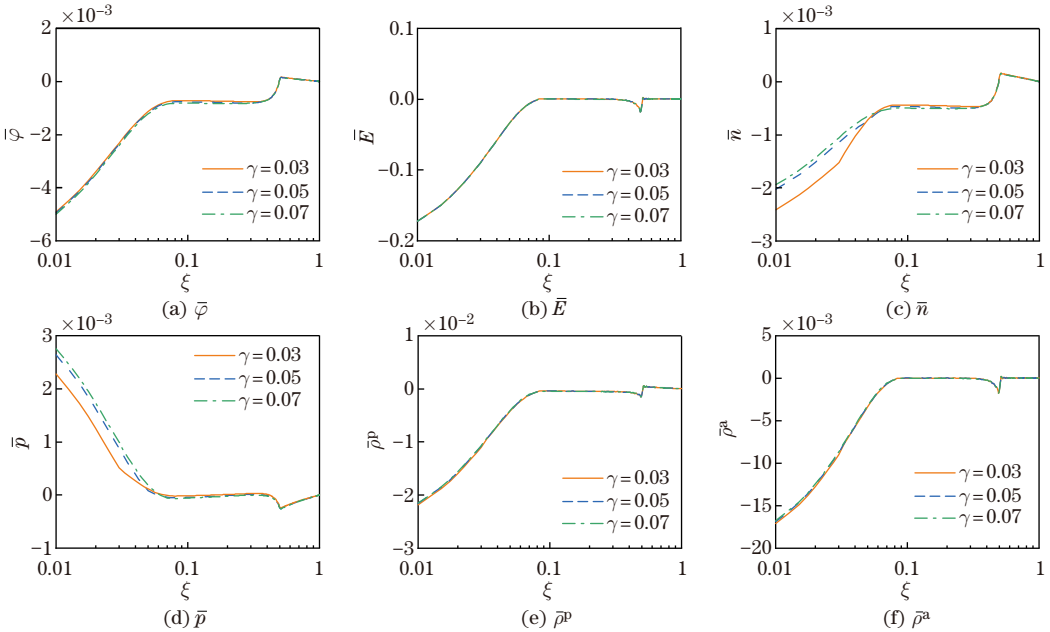

Fig. 6 Effects of the thickness ratio on the electrical properties (color online)

The non-dimensional total charge is expressed as $\overline{\rho}^{\mathrm{a}} = \overline{\rho}^{\mathrm{p}} + \overline{p} - \overline{n}$. From the calculated results, it can be found that the polarization charge is much larger than the carrier charge, indicating that the total charge is dominated by the polarization charge.

In order to figure out how the interface position changes the electrical properties thoroughly, the perturbation carrier density at the heating surface is studied. The effects of the initial carrier density on the electrical properties are shown in Figs. 7(a) and 7(b). It can be observed that $\overline{n}$ decreases while $\overline{p}$ increases. This is because of the increment in the bulk of p-type semiconductor. Here, the carrier charge $\overline{p}(0) - \overline{n}(0)$ is also investigated. Define $\overline{\rho}^e = \overline{p}(0) - \overline{n}(0)$. Figure 7(c) gives the relative carrier charge $\overline{\rho}^e/\overline{\rho}_1^e$, where $\overline{\rho}_1^e$ is the carrier charge, when $\gamma = 0.01$. In addition, the effects of the initial carrier density on the electrical properties are studied. When the initial carrier density increases, the perturbation carrier increases. However, because of the screening effect, the electric potential decreases (see Fig. 7(d)). Besides, it can also be found that the position of the interface corresponding to the minimum carrier charge is altered by the initial carrier density, and the position tends to move toward the surface. This is because the increment in the p-type perturbation carrier density is much faster than the increment in the n-type perturbation carrier density for larger initial carrier density. These conclusions can be the guidance for the design of P-N junction modified semiconductor structure.

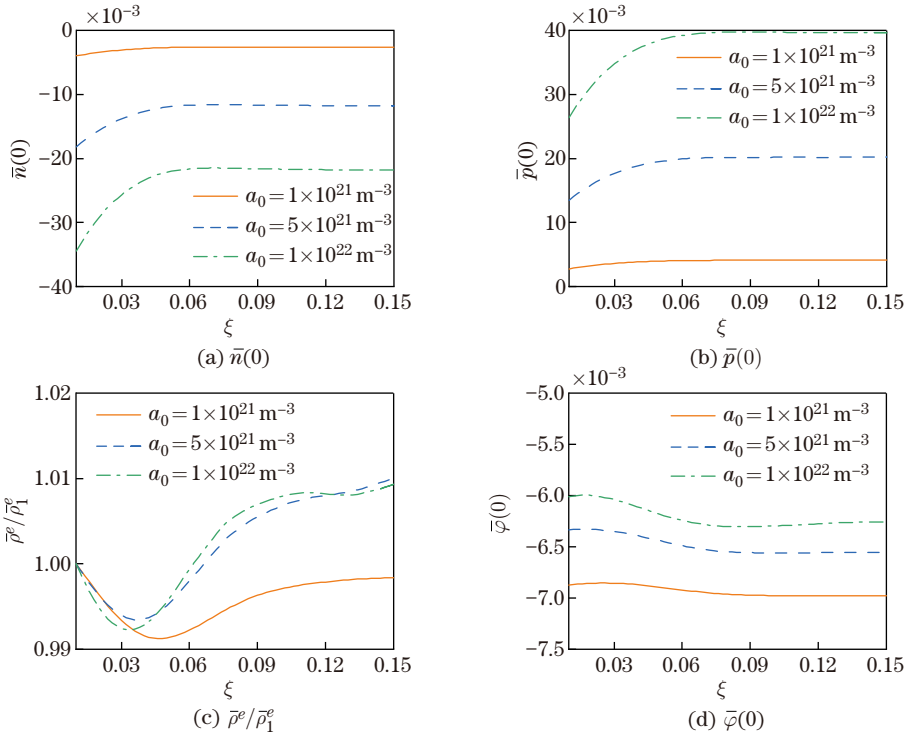

Fig. 7 Effects of the initial carrier density on the electrical properties for Case 2 (color online)

6 Conclusions

In this paper, the surface heating PS plate lying on a rigid substrate is investigated mathematically based on the thermo-electro-elastic coupling theory. The validity of derivation is illustrated by comparing the results from the analytical method and FEM. The surface heating induced mechanical or electrical responses are discussed in detail for three heating time. It is revealed that the maximum mechanical or electrical responses appear at the heating surface. The

investigations on the electric potential and the perturbation carrier density show that most carriers tend to concentrate in the zone near the heating surface, and longer heating time leads to greater screening effects on the electric potential. Besides, the values of mechanical or electrical field quantities with the consideration of thermal relaxation time are smaller than those without the consideration of thermal relaxation time. The slops of jumps at the elastic wavefront for the electric potential and perturbation carrier density are reduced. Furthermore, the effects of the interface position between the n-type and p-type plates on the electrical responses are studied. The conclusions in this article can be used to design thermoelectricity devices or solar cells.

References

[1] WANG, Z. L. Piezopotential gated nanowire devices: piezotronics and piezo-phototronics. *Nano Today*, **5**, 540–552 (2010)

[2] WU, W. and WANG, Z. L. Piezotronics and piezo-phototronics for adaptive electronics and optoelectronics. *Nature Reviews Materials*, **1**, 1–17 (2016)

[3] WANG, Z. L. and SONG, J. Piezoelectric nanogenerators based on zinc oxide nanowire arrays. *Science*, **312**, 242–246 (2006)

[4] HUANG, H., ZHANG, H., CAO, Y., LIU, Y., MA, K., LIU, K., and LIANG, Y. C. High-temperature three-dimensional GaN-based hall sensors for magnetic field detection. *Journal of Physics D*: *Applied Physics*, **54**, 075003 (2020)

[5] HAN, W., ZHOU, Y., ZHANG, Y., CHEN, C. Y., LIN, L., WANG, X., and WANG, Z. L. Correction to strain-gated piezotronic transistors based on vertical zinc oxide nanowires. *ACS Nano*, **6**, 5736–5736 (2012)

[6] YU, R., WU, W., DING, Y., and WANG, Z. L. GaN nanobelt-based strain-gated piezotronic logic devices and computation. *ACS Nano*, **7**, 6403–6409 (2013)

[7] WANG, Z. L. Nanobelts, nanowires, and nanodiskettes of semiconducting oxides — from materials to nanodevices. *Advanced Materials*, **15**, 432–436 (2003)

[8] ZHANG, C., WANG, X., CHEN, W., and YANG, J. An analysis of the extension of a ZnO piezoelectric semiconductor nanofiber under an axial force. *Smart Material Structures*, **26**, 025030 (2016)

[9] ZHANG, C. L., LUO, Y. X., CHENG, R. R., and WANG, X. Y. Electromechanical fields in piezoelectric semiconductor nanofibers under an axial force. *MRS Advances*, **2**, 3421–3426 (2017)

[10] ZHANG, C., WANG, X., CHEN, W., and YANG, J. Bending of a cantilever piezoelectric semiconductor fiber under an end force. *Generalized Models and Non-classical Approaches in Complex Materials* 2, Springer, Cham, 261–278 (2018)

[11] YANG, G., DU, J., WANG, J., and YANG, J. Extension of a piezoelectric semiconductor fiber with consideration of electrical nonlinearity. *Acta Mechanica*, **229**, 4663–4676 (2018)

[12] ZHAO, M. H., MA, Z. L., LU, C. S., and ZHANG, Q. Y. Application of the homopoty analysis method to nonlinear characteristics of a piezoelectric semiconductor fiber. *Applied Mathematics and Mechanics* (*English Edition*), **42**(5), 665–676 (2021) https://doi.org/10.1007/s10483-021-2726-5

[13] LI, P., JIN, F., and YANG, J. Effects of semiconduction on electromechanical energy conversion in piezoelectrics. *Smart Materials and Structures*, **24**, 025021 (2015)

[14] WANG, G., LIU, J., LIU, X., FENG, W., and YANG, J. Extensional vibration characteristics and screening of polarization charges in a ZnO piezoelectric semiconductor nanofiber. *Journal of Applied Physics*, **124**, 094502 (2018)

[15] LUO, Y., ZHANG, C., CHEN, W., and YANG, J. An analysis of PN junctions in piezoelectric semiconductors. *Journal of Applied Physics*, **122**, 204502 (2017)

[16] LUO, Y., CHENG, R., ZHANG, C., CHEN, W., and YANG, J. Electromechanical fields near a circular PN junction between two piezoelectric semiconductors. *Acta Mechanica Solida Sinica*, **31**, 127–140 (2018)

[17] FAN, S., YANG, W., and HU, Y. Adjustment and control on the fundamental characteristics of a piezoelectric PN junction by mechanical-loading. *Nano Energy*, **52**, 416–421 (2018)

[18] FAN, S., HU, Y., and YANG, J. Stress-induced potential barriers and charge distributions in a piezoelectric semiconductor nanofiber. *Applied Mathematics and Mechanics* (*English Edition*), **40**(5), 591–600 (2019) https://doi.org/10.1007/s10483-019-2481-6

[19] YANG, G., DU, J., WANG, J., and YANG, J. Electromechanical fields in a nonuniform piezoelectric semiconductor rod. *Journal of Mechanics of Materials and Structures*, **13**, 103–120 (2018)

[20] YANG, W., HU, Y., and PAN, E. Tuning electronic energy band in a piezoelectric semiconductor rod via mechanical loading. *Nano Energy*, **66**, 104147 (2019)

[21] CHENG, R., ZHANG, C., CHEN, W., and YANG, J. Piezotronic effects in the extension of a composite fiber of piezoelectric dielectrics and nonpiezoelectric semiconductors. *Journal of Applied Physics*, **124**, 064506 (2018)

[22] LUO, Y., ZHANG, C., CHEN, W., and YANG, J. Piezopotential in a bended composite fiber made of a semiconductive core and of two piezoelectric layers with opposite polarities. *Nano Energy*, **54**, 341–348 (2018)

[23] YANG, G., YANG, L., DU, J., WANG, J., and YANG, J. PN junctions with coupling to bending deformation in composite piezoelectric semiconductor fibers. *International Journal of Mechanical Sciences*, **173**, 105421 (2020)

[24] CHENG, R., ZHANG, C., ZHANG, C., and CHEN, W. Magnetically controllable piezotronic responses in a composite semiconductor fiber with multiferroic coupling effects. *Physica Status Solidi A*, **217**, 1900621 (2020)

[25] LIANG, C., ZHANG, C., CHEN, W., and YANG, J. Electrical response of a multiferroic composite semiconductor fiber under a local magnetic field. *Acta Mechanica Solida Sinica*, **33**, 663–673 (2020)

[26] KONG, D., CHENG, R., ZHANG, C., and ZHANG, C. Dynamic manipulation of piezotronic behaviors of composite multiferroic semiconductors through time-dependent magnetic field. *Journal of Applied Physics*, **128**, 064503 (2020)

[27] CHENG, R., ZHANG, C., and YANG, J. Thermally induced carrier distribution in a piezoelectric semiconductor fiber. *Journal of Electronic Materials*, **48**, 4939–4946 (2019)

[28] CHENG, R., ZHANG, C., CHEN, W., and YANG, J. Temperature effects on mobile charges in extension of composite fibers of piezoelectric dielectrics and non-piezoelectric semiconductors. *International Journal of Applied Mechanics*, **11**, 1950088 (2019)

[29] CHENG, R., ZHANG, C., CHEN, W., and YANG, J. Temperature effects on PN junctions in piezoelectric semiconductor fibers with thermoelastic and pyroelectric couplings. *Journal of Electronic Materials*, **49**, 3140–3148 (2020)

[30] CHENG, R., ZHANG, C., CHEN, W., and YANG, J. Electrical behaviors of a piezoelectric semiconductor fiber under a local temperature change. *Nano Energy*, **66**, 104081 (2019)

[31] YANG, Z., SUN, L., ZHANG, C., ZHANG, C., and GAO, C. Analysis of a composite piezoelectric semiconductor cylindrical shell under the thermal loading. *Mechanics of Materials*, **164**, 104153 (2022)

[32] FENG, Q., SHI, X., XING, Y., LI, T., LI, F., PAN, D., and LIANG, H. Thermoelectric microgenerators using a single large-scale Sb doped ZnO microwires. *Journal of Alloys and Compounds*, **739**, 298–304 (2018)

[33] DOU, Y., WU, F., FANG, L., LIU, G., MAO, C., WAN, K., and ZHOU, M. Enhanced performance of dye-sensitized solar cell using Bi_2Te_3 nanotube/ZnO nanoparticle composite photoanode by the synergistic effect of photovoltaic and thermoelectric conversion. *Journal of Power Sources*, **307**, 181–189 (2016)

[34] LORD, H. W. and SHULMAN, Y. A generalized dynamical theory of thermoelasticity. *Journal of the Mechanics and Physics of Solids*, **15**, 299–309 (1967)

[35] GREEN, A. E. and LINDSAY, K. A. Thermoelasticity. *Journal of Elasticity*, **2**, 1–7 (1972)

[36] XIONG, Q. L. and TIAN, X. G. Response of a semi-infinite microstretch homogeneous isotropic body under thermal shock. *Journal of Applied Mechanics*, **78**, 925–948 (2011)

[37] TANG, F. and SONG, Y. Wave reflection in semiconductor nanostructures. *Theoretical and Applied Mechanics Letters*, **8**, 160–163 (2018)

[38] CHANDRASEKHARAIAH, D. S. A generalized linear thermoelasticity theory for piezoelectric media. *Acta Mechanica*, **71**(1), 39–49 (1988)

[39] CHANDRASEKHARAIAH, D. S. A temperature-rate-dependent theory of thermopiezoelectricity. *Journal of Thermal Stresses*, **7**, 293–306 (1984)

[40] HE, T. H., SHEN, Y. P., and TIAN, X. G. A two-dimensional generalized thermal shock problem for a half-space in electromagneto-thermoelasticity. *International Journal of Engineering Science*, **42**, 809–823 (2004)

[41] LI, H. M., WANG, Y. M., WANG, B. Y., and HE, T. H. The dynamic response of a rotating thick piezoelectric plate with thermal relaxations. *Applied Mechanics and Materials*, **52**, 1565–1570 (2011)

[42] WAUER, J. and SUHERMAN, S. Thickness vibrations of a piezo-semiconducting plate layer. *International Journal of Engineering Science*, **35**, 1387–1404 (1997)

[43] SLADEK, J., SLADEK, V., PAN, E., and WÜNSCHE, M. Fracture analysis in piezoelectric semiconductors under a thermal load. *Engineering Fracture Mechanics*, **126**, 27–39 (2014)

[44] SZE, S. M. *Physics of Semiconductor Devices*, Wiley, Hoboken (1981)

[45] WU, W., YU, H., XUE, R., ZHAO, T., TAO, R., LIAO, H., and JI, Z. Efficient model for the elastic load of film-substrate system involving imperfect interface effects. *Theoretical and Applied Mechanics Letters*, **10**, 390–404 (2020)

[46] DURBIN, F. Numerical inversion of Laplace transforms: an efficient improvement to Dubner and Abate's method. *Computer Journal*, **17**, 371–376 (1974)

[47] SADAO, A. *Properties of Group*-IV, III-V, *and* II-VI *Semiconductors*, Wiley, Hoboken (2005)

[48] LI, C. L., GUO, H. L., TIAN, X. G., and HE, T. H. Generalized piezoelectric thermoelasticity problems with strain rate and transient thermo-electromechanical responses analysis. *Zeitschrift für Angewandte Mathematik und Mechanik*, **100**, e201900067 (2020)